© 1998 The Chemical Society of Japan

Hubbard and Heisenberg Models for Four-Site Four-Electron Systems. Group-Theoretical Interrelationships and Applications to Multinuclear Transition-Metal Clusters

Yasunori Yoshioka,* Shigehiro Kubo, Shinji Kiribayashi, Yu Takano, and Kizashi Yamaguchi*

Department of Chemistry, Graduate School of Science, Osaka University, Toyonaka, Osaka 560

(Received September 4, 1997)

Hubbard models for four-site four-electron {4,4} systems are analytically solved to elucidate group-theoretical interrelationships between effective model Hamiltonians for radical clusters, metal clusters, Cu_4O_4, and so on. The group operations used for this purpose are permutation group (S_N), spatial symmetry (P_N), spin rotation (S), and time-reversal (T). The magnetic (color) group ($T\times S$) is utilized for determination of the magnetic symmetry of spin structures obtained on the basis of the classical Heisenberg model; namely a vector representation of radical spins. The magnetic double group theory ($T\times S\times P_N$) is used for characterization of general Hartree–Fock solutions (GHF) involving axial, helical, and torsional spin density waves for {4,4} systems. The spin-optimized SCF solutions are constructed from the spin projection of the GHF solutions ($T\times S\times P_N$) by the use of the permutation symmetry (S_N). The S_N group is also used for the quantum Heisenberg model for {4,4} systems. In order to show the interrelationships between these model Hamiltonians, the electronic states of {4,4} systems with the D_{4h}, T_d, and D_{3h} symmetries are constructed by the use of the magnetically ordered general spin orbitals which have been determined by the GHF calculations. The spin-optimized SCF solutions for {4,4} systems examined here are equivalent to the full CI wavefunctions satisfying both spatial and spin symmetries. The relative contributions of the spin polarization (SP) and doubly excited configurations in the GHF, projected GHF and SO-SCF wavefunctions are clarified to elucidate possible mechanisms of spin alignments and antiferromagnetic spin correlations. Implications of these computational results are discussed in relation to quantum and classical representations of spin alignments in molecular magnetic materials such as iron–sulfur clusters. Molecular magnets having helical and torsional spin structures are designed and discussed in relation to the most general spin alignment in the species.

Several model Hamiltonians have been used for molecular systems with and without strong electronic correlations. Among them the Hubbard model[1] has been employed to elucidate variations of electronic properties of the species from the weak correlation regime to the strong correlation limit in combination with the generalized Hartree–Fock (GHF) and configuration interaction (CI) methods.[2] The valence-bond (VB) type model[3] is often utilized in the strong correlation regime for treating spin correlation effects in radical species. It is particularly useful for derivation of selection rules for radical reactions.[4,5] On the other hand, the VB selection rule derived from the classification of the starred (*) and unstarred carbon atoms in alternant hydrocarbons is applicable to prediction of possible high- and low-spin ground states of organic polyradicals.[6] Thus selection rules for spin-related phenomena are easily derived on the basis of the quantum Heisenberg (QHB) model, which is one of the simplest VB models.[4,5,7]

$$H(\mathrm{QHB}) = -\sum 2J_{ab}\boldsymbol{S}_a\cdot\boldsymbol{S}_b, \qquad (1)$$

where J_{ab} is the effective exchange integral and $\boldsymbol{S}_c$ (c=a,b) denotes spin at the site c. The QHB model is also utilized for description of magnetic behaviors observed for multicenter transition metal complexes such as copper oxides. On the other hand, spin alignments and/or spin correlations are pictorially expressed by the classical arrow notations for localized electrons in the classical Heisenberg (CHB) model.[8,9]

$$H(\mathrm{CHB}) = -\sum 2J_{ab}S_aS_b\cos\theta_{ab}, \qquad (2)$$

where θ_{ab} means the angle between the spin vectors and S_c (c=a,b) is the magnitude of spin. Since spin alignments often have magnetic symmetries, spin alignment rules are described in terms of the magnetic group, which is given by the direct product of the spin rotation (S) and time reversal (T).[10] The T-operation is necessary for the spin inversion because spin is an axial vector instead of a polar vector. Penney's bond order,[11] which is given by the scalar product of spin vectors in Eq. 2, is used for description of the spin coupling. For example, a negative ($\theta_{ab}>90°$) value means the singlet-type spin coupling or correlation. Therefore, the Penney's bond order in quantum chemistry is nothing but the spin correlation function K_{ab} in solid state physics.[12]

The spin alignment rules are also derived from the Hartree–Fock (HF) MO-theoretical model.[13] The spin alignments are closely related to the instabilities[14] of the HF solutions in the molecular orbital (MO) approach. In previous papers,[15,16] the instability conditions for the restricted Hartree–Fock (RHF) solutions for doublet and triplet states have been formulated and applied to three- and four-elec-

tron systems which are of basic importance for theoretical understanding of spin alignments. It was shown that the instability conditions for the doublet[15] and triplet[16] solutions as well as singlet RHF solution are useful for the examination of the orbital and spin degeneracy problems in molecular magnets. More stable generalized Hartree–Fock (GHF) solutions,[17—19] which involve two-component spinors, have been constructed on the basis of the instability matrices. The correlation effects incorporated with the GHF solutions were analyzed in relation to the spin correlation (SC) function K_{SC} defined previously.[12] It was shown that the spin structures in the classical Heisenberg model are closely related to patterns of the K_{SC} functions of GHF solutions for species with strong correlation. The interrelationship between spin structures in the Heisenberg model and spin densities of the GHF solutions is also clarified from the viewpoint of the magnetic group theory.[10]

Although the GHF solutions involve important correlation effects in molecular magnets, they do not have correct symmetry properties.[20—23] Therefore, wavefunctions possessing pure symmetry properties are necessary to confirm the reliability of the GHF approximation.[21] Thus, the symmetry projection procedure has been an important problem in the GHF theory. We have already demonstrated that the spin-optimized (SO) SCF wavefunction of the three-center three-electron {3,3} system can be derived from the projection of the axial (**1**,**2**) and helical (**3**) spin density wave (ASDW and HSDW) solution with the triangular spin alignment (Chart 1).[23] The HSDW solution is written in the general spin orbitals (GSO): two-component spinors. There is no energy barrier on the hypersurface for the SO-SCF process starting from the symmetry-projected HSDW solution. Therefore, the HSDW solution is a good starting point to get correlated wavefunctions with correct symmetry properties. Generally, the SO-SCF wavefunctions constructed from the orthogonalized general spin orbitals are rewritten in the form of the complete active space (CAS) SCF wavefunction by the use of GHF natural orbitals (NO).[24—26] Judging from the rapid SCF convergence in the case of the {3,3} radical, we conclude that the natural orbitals and their occupation numbers derived from the HSDW solution should be good trials for the CASSCF calculations. Similar convergence behavior has been demonstrated in the case of the axial spin density wave (ASDW) solution for biradical species; ASDW with M_z-spin modulation is equivalent to the conventional UHF solution in quantum chemistry.

Recently systems having strong electron correlations have received great interest in relation to magnetic properties, together with spin-mediated superconductivity. The Hubbard models[1] are often utilized to elucidate general tendencies depending on the strength of electron correlation. The purpose of the present articles is to obtain both qualitative and quantitative pictures for electronic states of four-center four-electron {4,4} systems, which are considered as possible models for radical clusters, metal clusters, Cu_4O_4 cluster in cuprates, and so on. For the purpose, the spatial-symmetry-adapted wavefunctions from the orthogonalized GSOs are derived from the instability analysis of four-electron systems; the spin polarization (SP) and electron correlation (EC) effects involved in the systems can then be discussed. We consider the singlet and triplet states of the four-site four-electron {4, 4} models with the D_{4h} and T_d conformations and the triplet state with the D_{3h} conformation. In order to explain the interrelationship between the effective model Hamiltonians, the orbital set induced by the instability condition is characterized by the magnetic point group. It will be shown that the GHF solutions for the D_{4h}- and T_d-conformations have the D_{4h}- and T_d-magnetic symmetries, respectively. The projection on the pure S^2 and S_z components is achieved by using the previous projection procedure.[21—23] Each symmetry-adapted wavefunction obtained here possesses the correct spatial symmetry and is identical with the exact full CI solution within the active magnetic orbitals. These calculated results will be discussed in relation to the interrelationships between effective model Hamiltonians. Implications of the calculated results will be discussed on the basis of the relative contributions of the SP and EC effects and spin alignments in molecular magnets. Helical and torsional spin structures in multinuclear transition-metal complexes such as vanadium oxides and iron-sulfur complexes will also be proposed as the most general magnetic states in molecular magnetism.

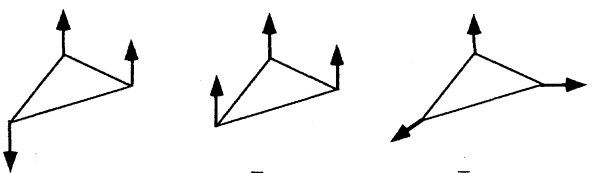

1 (m' m 2') **2** ($\bar{6}$ m' 2') **3** ($\bar{6}$' m' 2)

Chart 1.

Theoretical Backgrounds

Symmetry. The spin-free Hamiltonians H_{SF} commute with the symmetry elements of time-reversal (T), spin rotation (S), point group (P_N), and permutation (S_N) group.[27]

$$[H_{SF}, X] = 0, \quad X = T, S, P_N, S_N. \tag{3}$$

Hence, these four symmetry operations may be useful for considerations of the relations between the solutions of the effective Hamiltonians.[23] The quantum Heisenberg Hamiltonian involves only the spin variable. Therefore, it can be completely characterized by the permutation group S_N. Since in the case of spin clusters various VB structures belong to the irreducible representations of the permutation group, the spin couplings between the components can be expressed in terms of the S_N group. The classical Heisenberg model, on the other hand, treats the spin moments whose mutual directions are utilized to express the spin structures in the clusters. The magnetic point group M_N will be useful for their characterization:[10]

$$M_N = H_N + T(P_N - H_N), \tag{4}$$

where H_N is a subgroup of P_N.

For general spin orbitals, there are three different symmetry operations: (i) time-reversion, T, (ii) spin rotation, S, and (iii) spatial symmetry operation, P_N. Therefore, any orbital set belongs to the irreducible representation of a subgroup of the direct product group, $T\times S\times P_N$.[18] In most cases, the ground GHF spin orbitals have the full symmetry of the direct product group. Thus in the GHF theory, spin alignments can well be characterized by both spin ($T\times S$) and space (P_N) symmetries. An extended Hartree–Fock wavefunction can be constructed by use of the direct product group $G=S_N\times T\times S\times P_N$.[21] The group-theoretical relationships between the solutions of various model Hamiltonians are diagrammatically illustrated in Fig. 1.

Spin Structures. Here, the notations of spin structures are briefly summarized. Figure 2 illustrates schematically the axial, helical, and torsional spin structures, which have one, two, and three dimensional spin components, respectively.[18,19] The Hartree–Fock (HF) solution with the 1D spin structure is called as the axial spin density wave (ASDW) as illustrated in Fig. 2A. The ASDW solution can be further classified into three groups on the basis of directions (X, Y, and Z) of spin vector. The ASDW with the Z-axis spin modulation (ASDWZ) is the usual UHF solution. The HF solutions with the 2D and 3D spin structures are denoted as the helical spin density wave (HSDW) and torsional spin wave (TSW), respectively.

Before the construction of GHF solution, the classical Heisenberg model provides possible spin alignments characterized by the magnetic group ($T\times S$). Here, the GHF solution in Fig. 1 is constructed to elucidate the interrelationships between these model Hamiltonians. General methods of the symmetry projections for the GHF solutions have already been discussed in previous papers.[23] In the case of the present $\{4,4\}$ system, there are four magnetically ordered general spin orbitals (GSO). The wavefunction which has the pure spin symmetry is to be derived as

$$^{2S+1}\Psi = P_{S^2}P^M_{S_z}\psi_1\psi_2\psi_3\psi_4, \tag{5}$$

where $P^M_{S_z}$ is the projection operator extracting the eigenfunction of S_z with the desired eigenvalue M.[23] The projection operator P_{S^2} [28–30] extracting the desired $\langle S^2\rangle = S(S+1)$ is given by the Wigner operators[27] acting on the spin and spatial coordinates, respectively. We carry out the projections with $P^M_{S_z}$ and P_{S^2} as indicated in Eq. 5 and subsequently normalize the wavefunction. The wavefunction (Eq. 5), which has been optimized with respect to both the spin coupling coefficients and orbital-mixing parameters, is the spin-optimized self-consistent-field (SO-SCF) wavefunction of our present concern. The SO-SCF wavefunction obtained here is equivalent to the complete active space (CAS) SCF solution by the use of active magnetic orbitals and magnetic electrons. Table 1 summarizes the notations of several wavefunctions used in this paper.

Table 1. Notations for Wavefunctions Employed

Notations	Full name
GHF	Generalized Hartree-Fock (HF)
ASDWQ	Axial spin density wave with M_Q-spin modulation (Q=X, Y, Z)
PSDW	Projected SDW
EHF	Extended HF, i.e., SCF solution after the projection of SDW by Löwdin procedure
SO-SCF	Spin-optimized SCF

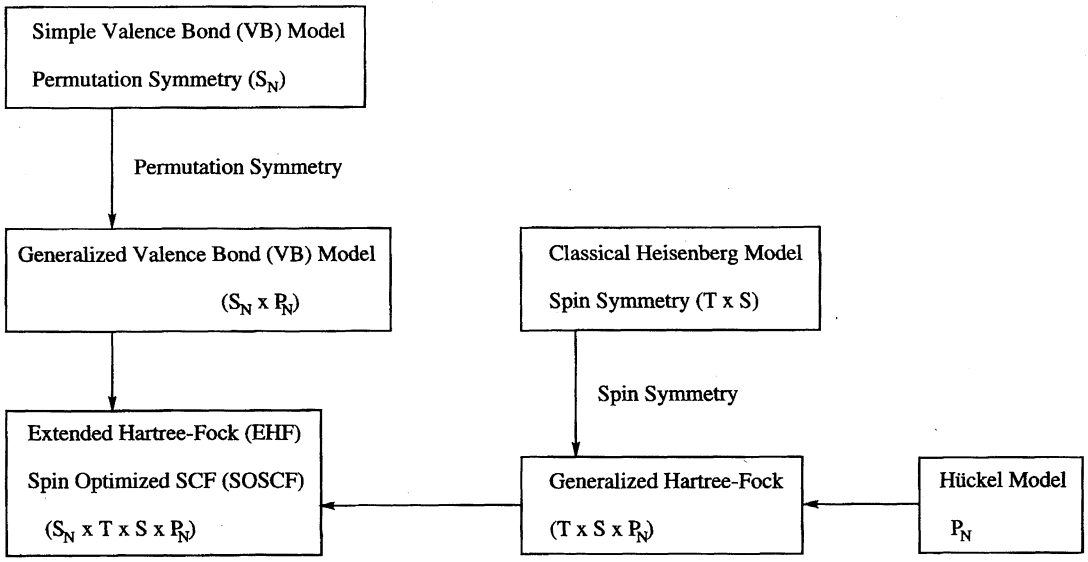

Fig. 1. Schematic illustrations of the effective model Hamiltonians used for calculations of electronic structures of molecular systems. The model Hamiltonians are characterized by the symmetry elements of time-reversal (T), spin rotation (S), point group (P_N), and permutation (S_N) group.

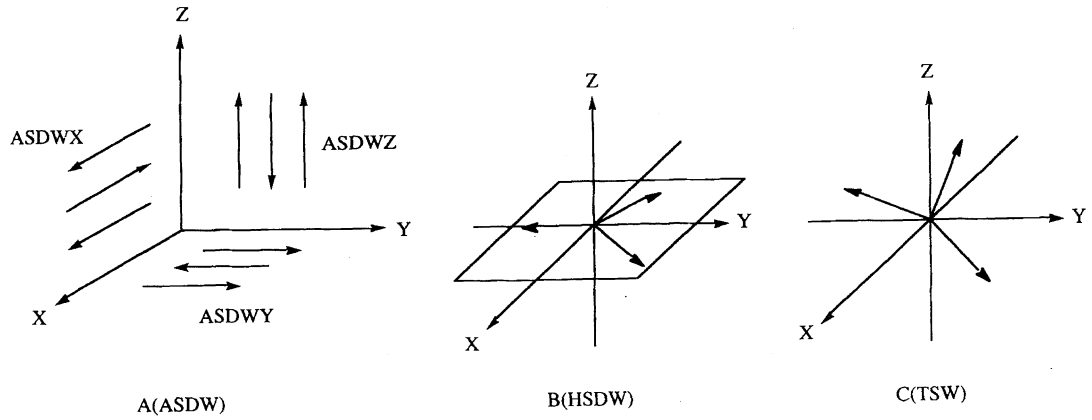

Fig. 2. Schematic illustrations of the spin alignments; (A) axial spin density wave (ASDW) solutions with the x, y, and z-spin modulation; (B) helical SDW (HSDW) solution with two-dimensional spin modulation in the xy-plane; (C) tortional spin wave (TSW) solution with the three-dimensional spin modulation.

SO-SCF Calculations of Four-Site Models

Singlet State in the D_{4h} Conformation. There are several molecular systems with D_{4h} conformation: H_4 cluster (**4**), cyclobutadiene (**5**), Cu_4O_4 cluster (**6**) in cuprates, and so on (Chart 2). The electronic structures for these systems are approximated by the {4,4} Hubbard model, which can be solved analytically. The RHF orbitals $\{\phi_i\}$ are given by the D_{4h} spatial symmetry as[16]

$$\begin{pmatrix} \phi_1 \\ \phi_2 \\ \phi_3 \\ \phi_4 \end{pmatrix} = \frac{1}{2}\begin{pmatrix} 1 & 1 & 1 & 1 \\ 1 & 1 & -1 & -1 \\ 1 & -1 & -1 & 1 \\ 1 & -1 & 1 & -1 \end{pmatrix}\begin{pmatrix} \chi_1 \\ \chi_2 \\ \chi_3 \\ \chi_4 \end{pmatrix}, \quad (6)$$

where, χ_p is the orthonormalized atomic orbital on site p. The orbitals ϕ_1 and ϕ_4 have the symmetries, a_{1g} and b_{2g}, respectively, and ϕ_2 and ϕ_3 are the bases of e_u symmetry. The instability condition for singlet RHF solution gives the M_z-modulated (**7**) axial spin-density-wave (ASDWZ) solution (Chart 3): namely the traditional singlet UHF solution used in quantum chemistry.

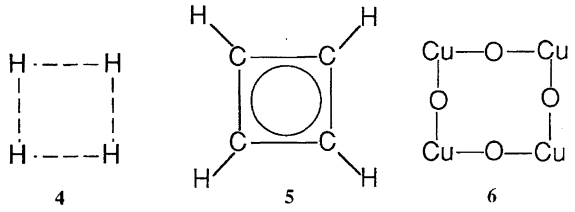

4 5 6

Chart 2.

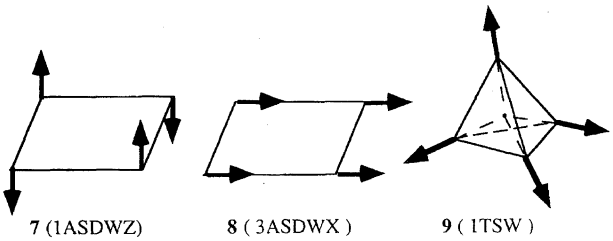

7 (1ASDWZ) 8 (3ASDWX) 9 (1TSW)

Chart 3.

$$\psi_1^{\pm} = \left[\left(\cos\frac{\lambda}{2}\right)\phi_1 \pm \left(\sin\frac{\lambda}{2}\right)\phi_4\right]\eta_{\pm}, \quad (7)$$
$$\psi_2^{\pm} = \frac{1}{\sqrt{2}}(\phi_2 \pm \phi_3)\eta_{\pm},$$

and the wavefunction of ASDWZ solution is given as

$$^1\Psi_{ASDWZ} = |\psi_1^+\psi_1^-\psi_2^+\psi_2^-|, \quad (8)$$

where η_+ and η_- are the α- and β-spin functions, respectively. the different-orbitals-for-different-spins (DODS) type MOs in Eq. 7 are schematically depicted in Ref. 8. The reduced total electronic energy depends on the orbital mixing parameter λ:

$$^1\tilde{E}_{ASDWZ} = -4x\cos\lambda - \frac{1}{4}\sin^2\lambda - \frac{1}{2}\sin\lambda + \frac{3}{4}, \quad (9)$$

where x is the ratio of the resonance integral, β (or transfer integral, $-t$) to the on-site repulsion integral $U=\langle\chi_p\chi_p|\chi_p\chi_p\rangle$:

$$x = -\frac{\beta}{U} = \frac{t}{U}. \quad (10)$$

Also, $\tilde{E}_R$ is the reduced (dimensionless) energy of a given state R defined as

$$\tilde{E}_R = (E_R - 4\alpha)/\beta, \quad (11)$$

where α is the coulomb integral.

Table 2 shows the transformation properties of the ASDWZ solution. The ASDWZ state is kept invariant under the symmetry operations of the subgroup D_{2h} (= H_N in Eq. 4) of the point group D_{4h}. Under the elements of (D_{4h}–D_{2h}) with the time reversal operation, the ASDWZ state is also invariant. Therefore, the ASDWZ solution is the magnetically ordered set which possesses the symmetry characterized as the magnetic point group $4'/mmm'$.[10]

Since the orbital product $\psi_1^+\psi_1^-\psi_2^+\psi_2^-$ is already the eigenfunction with $M=0$ of the operator S_z^0, we project $\psi_1^+\psi_1^-\psi_2^+\psi_2^-$ on the pure state with the eigenvalue $\langle S^2\rangle=0$ by means of Eq. 5. The explicit form of the projected wavefunction can be compactly written in a linear combination of the spin-restricted configurations:

Table 2. Transformation Properties of the ASDWZ Orbitals with the $4'/mmm'$ Symmetry[a,b]

	E	$(C_{4z}^{+})^t$	$(C_{4z}^{-})^t$	C_{2z}	C_{2x}	C_{2y}	$(C_{2a})^t$	$(C_{2b})^t$
Ψ_1^+	Ψ_1^+	$-\varepsilon^*\Psi_1^-$	$-\varepsilon\Psi_1^-$	$-i\Psi_1^+$	$-i\Psi_1^-$	Ψ_1^-	$\varepsilon^*\Psi_1^+$	$\varepsilon\Psi_1^+$
Ψ_1^-	Ψ_1^-	$\varepsilon\Psi_1^+$	$\varepsilon^*\Psi_1^-$	$i\Psi_1^-$	$-i\Psi_1^+$	$-\Psi_1^+$	$\varepsilon\Psi_1^-$	$\varepsilon^*\Psi_1^-$
Ψ_2^+	Ψ_2^+	$-\varepsilon^*\Psi_2^-$	$\varepsilon\Psi_2^-$	$i\Psi_2^+$	$i\Psi_2^-$	Ψ_2^-	$\varepsilon^*\Psi_2^+$	$-\varepsilon\Psi_2^+$
Ψ_2^-	Ψ_2^-	$-\varepsilon\Psi_2^+$	$\varepsilon^*\Psi_2^-$	$-i\Psi_2^-$	$i\Psi_2^+$	$-\Psi_2^+$	$-\varepsilon\Psi_2^-$	$\varepsilon^*\Psi_2^-$
	I	$(S_{4z}^{-})^t$	$(S_{4z}^{+})^t$	σ_z	σ_x	σ_y	$(\sigma_{da})^t$	$(\sigma_{db})^t$
Ψ_1^+	Ψ_1^+	$-\varepsilon^*\Psi_1^-$	$-\varepsilon\Psi_1^-$	$-i\Psi_1^+$	$-i\Psi_1^-$	Ψ_1^-	$\varepsilon^*\Psi_1^+$	$\varepsilon\Psi_1^+$
Ψ_1^-	Ψ_1^-	$\varepsilon\Psi_1^+$	$\varepsilon^*\Psi_1^+$	$i\Psi_1^-$	$-i\Psi_1^+$	$-\Psi_1^+$	$\varepsilon\Psi_1^-$	$\varepsilon^*\Psi_1^-$
Ψ_2^+	$-\Psi_2^+$	$-\varepsilon^*\Psi_2^-$	$-\varepsilon\Psi_2^-$	$-i\Psi_2^+$	$-i\Psi_2^-$	$-\Psi_2^-$	$-\varepsilon^*\Psi_2^+$	$\varepsilon\Psi_2^+$
Ψ_2^-	$-\Psi_2^-$	$-\varepsilon\Psi_2^+$	$-\varepsilon^*\Psi_2^+$	$i\Psi_2^-$	$-i\Psi_2^+$	Ψ_2^+	$\varepsilon\Psi_2^-$	$-\varepsilon^*\Psi_2^-$

a) $\varepsilon=\exp(\frac{\pi}{4}i)$. b) t is a time inversion operator.

$$^1\Psi_{\text{ASDWZ-SO-SCF}} = D_1\Phi_G^s + D_2\Phi_{SP}^s + D_3\Psi_{DE}^s, \quad (12)$$

where

$$\Phi_G^s = \frac{1}{\sqrt{2}}(|\phi_1\overline{\phi}_1\phi_2\overline{\phi}_2| - |\phi_1\overline{\phi}_1\phi_3\overline{\phi}_3|),$$
$$\Phi_{SP}^s = \frac{1}{2\sqrt{3}}(|\phi_1\overline{\phi}_2\phi_3\overline{\phi}_4| + |\overline{\phi}_1\phi_2\overline{\phi}_3\phi_4| + |\phi_1\phi_2\overline{\phi}_3\overline{\phi}_4| + |\overline{\phi}_1\overline{\phi}_2\phi_3\phi_4| - 2|\phi_1\overline{\phi}_2\overline{\phi}_3\phi_4| - 2|\overline{\phi}_1\phi_2\phi_3\overline{\phi}_4|), \quad (13)$$
$$\Phi_{DE}^s = \frac{1}{\sqrt{2}}(|\phi_2\overline{\phi}_2\phi_4\overline{\phi}_4| - |\phi_3\overline{\phi}_3\phi_4\overline{\phi}_4|),$$

and where the CI coefficient D_i (i=1—3) is expressed with the normalizing factor (N), the orbital mixing parameter (λ), and the spin coupling coefficients C_i (i=1,2):

$$D_1 = \frac{C_2N}{\sqrt{2}}\cos^2\frac{\lambda}{2}, \quad D_2 = \frac{\sqrt{3}}{6}C_2N\sigma\sin\lambda,$$
$$D_3 = -\frac{C_2N}{\sqrt{2}}\sin^2\frac{\lambda}{2},$$
$$\left(\frac{C_2N}{2}\right)^2 = \left[2+\left(\frac{\sigma^2}{3}-1\right)\sin^2\lambda\right]^{-1}, \quad (14)$$
$$\sigma = \frac{C_1}{C_2}.$$

Φ_G^s, Φ_{SP}^s, and Φ_{DE}^s are the ground (G), spin-polarization (SP), and doubly-excited (DE) configurations, respectively, since the reference configuration Φ_G involves the two Slater determinants which are degenerate in energy. When the spin coupling parameter σ is taken to be equal to unity, the SO-SCF wavefunction (Eq. 12) is reduced to the spin-extended HF (EHF) solution by Löwdin.[20c]

The configurations Φ_G, Φ_{SP}, and Φ_{DE} possess the common space symmetry B_{1g}. Namely, the projection improves the space symmetry as well as the spin symmetry. The SO-SCF function obtained here is nothing but the CASSCF solution, which is equivalent to the full CI solution within the four magnetic orbitals, since there are only three configurations of the B_{1g}-symmetry in the singlet state of the D_{4h} conformation.[31]

The reduced energy $^1\tilde{E}_{\text{SO-SCF}}$ calculated by Eq. 12 is as follows:

$$^1\tilde{E}_{\text{ASDWZ-SO-SCF}} = -4x(D_1^2 - D_3^2) + 3D_2^2/4 - \sqrt{6}D_2(D_1 - D_3)/2 + D_1D_3/2 + 3/4. \quad (15)$$

When σ=1,

$$^1\tilde{E}_{\text{PASDWZ}} = -\frac{24x\cos\lambda + 3\sin\lambda}{2(3-\sin^2\lambda)} + 3/4. \quad (16)$$

The energies of the RHF, ASDWZ (UHF), symmetry-projected ASDWZ (PASDWZ=PUHF), and SO-SCF (full CI) states are depicted in Fig. 3. The spin-extended HF (ASDWZ-EHF) state[23] exists between the SO-SCF and PASDWZ states. At the strong correlation limit (x=0) all the energies except for the RHF state converge to the energy of the four isolated spin fragments with S=1/2. The behavior of the ASDWZ state is similar to that of the SO-SCF state. Therefore, the ASDWZ state, namely singlet UHF, may be regarded as a fairly good approximation to the SO-SCF in

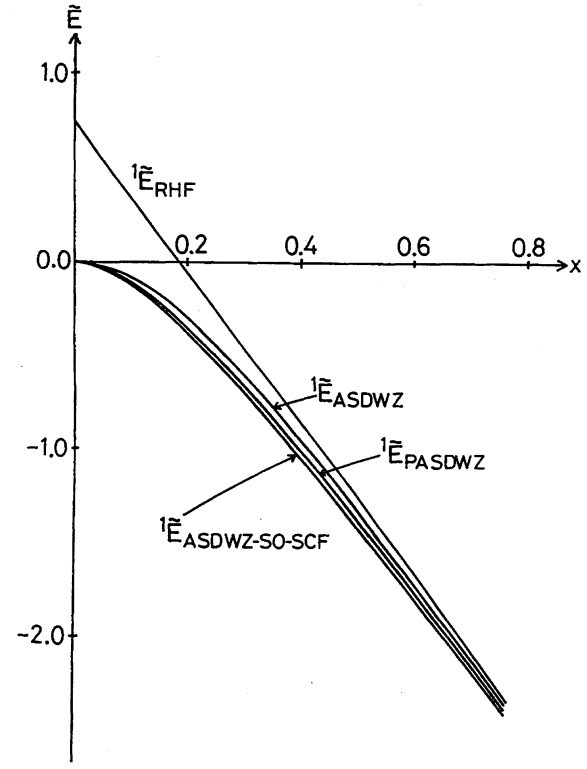

Fig. 3. Normalized energies of the ASDWZ-SO-SCF, spin-projected ASDWZ (PADWZ), ASDWZ, and RHF states of the singlet state in the D_{4h} conformation. In the T_d conformation, ASDW is replaced by TSW.

energy although it is symmetry-broken.

Figures 4(A) and 4(B) show the orbital mixing parameter λ and the spin coupling parameter σ, respectively. The λ-value of the ASDWZ-EHF state is larger than that of the ASDWZ state at any given x. When the spin degeneracy is taken into account, the λ-value increases further. As compared to λ, the σ-value is less sensitive to the variation of x. The spin-polarization (SP) effect tends to increase as the ASDWZ state is shifted to the EHF state by the optimization of λ. The double-excitation configuration becomes important, when the spin-coupling parameter σ is involved.

Shown in Fig. 5 is the tetraradical character (y)[16] calculated from the weights of Φ_{SP} and Φ_{DE}:

$$y = 2\left(D_2^2 - \frac{2}{3}D_3^2\right) = \frac{2}{3}\left(\frac{C_2N}{2}\right)[\sigma^2\sin^2\lambda + (1-\cos\lambda)^2]. \quad (17)$$

The tetraradical character of the EHF state nearly coincides with that of the SO-SCF state, and hence has been omitted in Fig. 5. The spin-polarization (SP) and double-excitation (DE) effects are underestimated in the PASDWZ state as compared with the SO-SCF solution. However the PASDWZ state is a very good trial for the SO-SCF solution since these differences are negligible. In the EHF state, the spin-polarization effect is overestimated, while the double-excitation effect is underestimated. These errors are corrected by taking the spin degeneracy into consideration. Thus it is noteworthy that the ASDWZ (UHF) and EHF solution more or less overestimate the SP contribution as compared with the SO-SCF (full CI) solution, and that the SP parameter defined in UHF and EHF should involve contribution of double excitation (electron correlation) effect in a renormalized manner.

Triplet State in the D_{4h} Conformation. For the triplet state, we obtain the M_x-modulated (**8**) ASDW (ASDWX) solution[16] from the spin-flipping instability conditions of the RHF solution:

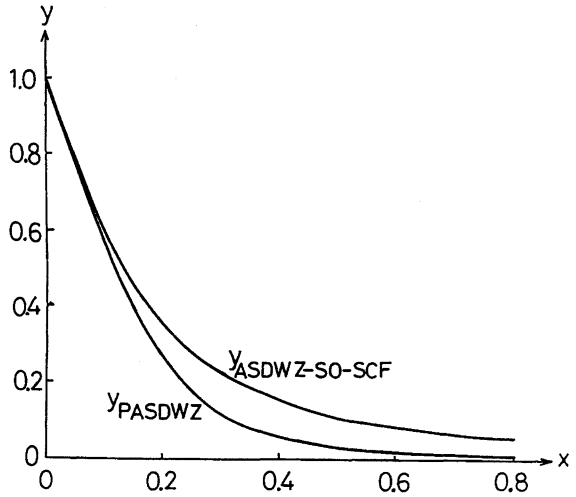

Fig. 5. Tetraradical character of the PASDWZ and ASDWZ-SO-SCF states of the singlet state in the D_{4h} conformation. In the T_d conformation, ASDWZ is replaced by TSW at the T_d conformation.

$$\psi_1^{\pm} = \left(\cos\frac{\lambda}{2}\right)\phi_1\eta_{\pm} + \left(\sin\frac{\lambda}{2}\right)\phi_4\eta_{\mp},$$
$$\psi_2^{\pm} = \frac{1}{2}(\phi_2\eta_{\pm} + \phi_3\eta_{\mp}). \quad (18)$$

The electronic energy ${}^3\tilde{E}_{ASDWX}$ of the Slater determinant constructed from the ASDWX solution is found to coincide with ${}^1\tilde{E}_{ASDWZ}$ (Eq. 9) under the Hubbard model.

The transformation properties of the ASDWX solution are characterized by the point group D_{2h} rather than D_{4h}. The ASDWX state is invariant under all elements of the subgroup C_{2h} of D_{2h}. Nor does it alter under the elements of $(D_{2h}-C_{2h})$ with the time reversal operation. Therefore, the ASDWX state of the triplet state possesses the symmetry represented by the magnetic point group $m'm'm$.

The P_{S^2}-projection of the orbital product $\psi_1^+\psi_1^-\psi_2^+\psi_2^-$ on the eigenstate with S=1 produces two spin coupling parame-

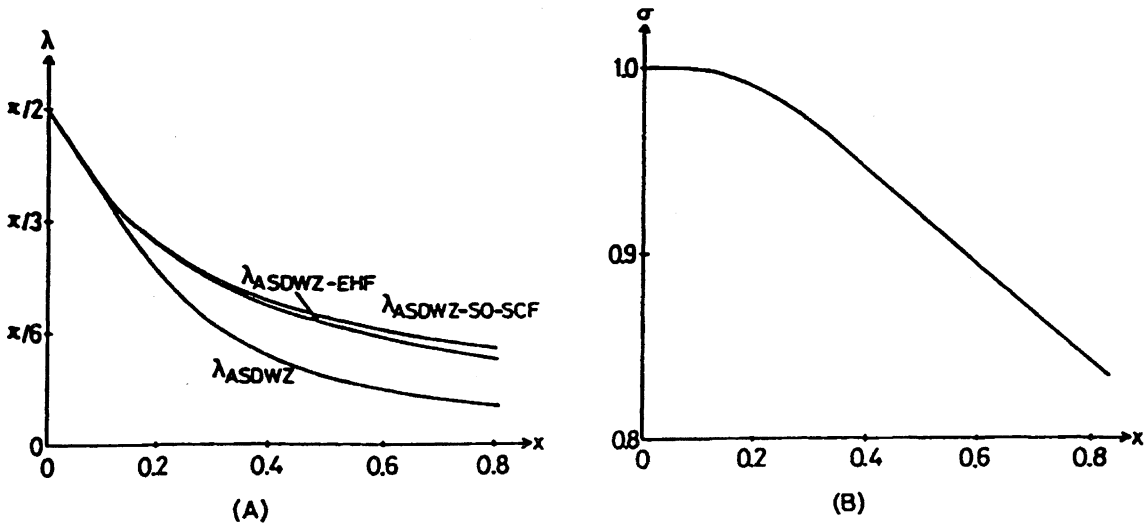

Fig. 4. (A) Variations of the orbital mixing parameter λ with x for the ASDWZ-SO-SCF, ASDWZ-EHF, and ASDWZ solutions for the singlet state in the D_{4h} conformation. (B) Variation of the spin coupling parameter σ with x for the ASDWZ-SO-SCF state.

ters $\sigma=C_1/C_3$ and $\tau=C_2/C_3$. It, therefore, is noteworthy that three spin coupling parameters are necessary for the triplet state of four spin systems. In this conformation, however, τ proves to equal σ under the variational condition for the energy. Therefore, the SO-SCF wavefunction of the triplet state is given as

$$^3\Psi_{\text{ASDWX-SO-SCF}} = D_1\Phi^{\text{t}}_{\text{GT}} + D_2\Phi^{\text{t}}_{\text{SI}} + D_3\Phi^{\text{t}}_{\text{DE}}, \tag{19}$$

where $\Phi^{\text{t}}_{\text{GT}}$, $\Phi^{\text{t}}_{\text{SI}}$, and $\Phi^{\text{t}}_{\text{DE}}$ denote the lowest-energy, semi-internal, and doubly-excited triplet configurations, respectively:

$$\begin{aligned}
\Phi^{\text{t}}_{\text{GT}} &= |\phi_1\overline{\phi}_1\phi_2\phi_3|,\\
\Phi^{\text{t}}_{\text{SI}} &= \frac{1}{\sqrt{2}}(|\phi_1\phi_2\overline{\phi}_2\phi_4| - |\phi_1\phi_3\overline{\phi}_3\phi_4|),\\
\Phi^{\text{t}}_{\text{DE}} &= |\phi_2\phi_3\phi_4\overline{\phi}_4|
\end{aligned} \tag{20}$$

and where the CI coefficients (D_i) are given by

$$\begin{aligned}
&D_1 = \frac{NC_3}{2}\cos^2\frac{\lambda}{2}, \quad D_2 = \frac{\sqrt{2}}{4}NC_3\sigma\sin\lambda\\
&D_3 = -\frac{NC_3}{2}\sin^2\frac{\lambda}{2}, \quad \left(\frac{NC_3}{2}\right)^2 = \left[1+\frac{1}{2}(\sigma^2-1)\sin^2\lambda\right]^{-1}.
\end{aligned} \tag{21}$$

These configurations $\Phi^{\text{t}}_{\text{GT}}$, $\Phi^{\text{t}}_{\text{SI}}$, and $\Phi^{\text{t}}_{\text{DE}}$ have the common space symmetry A_{2g}. Since there are only three configurations of the A_{2g} symmetry in the triplet state of the D_{4h} conformation, the ASDWX-SO-SCF solution should be identical with the full MC-SCF (full CI) solution. The situation indicates that the $P^1_{S_z}$ and P_{S^2} projections of the orbitals which have the symmetry of the magnetic point group $m'm'm$ produce the exact solution without the healing of the space symmetry.

The total electronic energy of the SO-SCF state is expressed in terms of the CI coefficients as

$$\begin{aligned}
^3\tilde{E}_{\text{ASDWX-SO-SCF}} = &-4x(D_1^2 - D_3^2)\\
&-D_2^2/4 - D_2(D_1 - D_3)/\sqrt{2}\\
&+D_1D_3/2 + 3/4.
\end{aligned} \tag{22}$$

The reduced energy for the case of $\sigma=1$ agrees with that of the ASDWX solution, so that the PASDWX and EHF states are identical with each other. The energies of the RHF, ASDWX, and SO-SCF (full CI) states are depicted in Fig. 6. The ASDWX state possessing the symmetry $m'm'm$ is a particularly good approximation to the exact full CI triplet solution. The lowering of the SO-SCF energy from the ASDWX energy is less than that of the singlet state. This in turn indicates that, since $^1\tilde{E}_{\text{ASDWZ}}=^3\tilde{E}_{\text{ASDWX}}$, the ground state of the D_{4h} conformation should be the singlet state, in agreement with the conclusion reached from the previous CI[31] calculations.

The familiar ASDWZ solution; triplet UHF solution, can be easily constructed from the DODS MOs in Eq. 7 as

$$^3\Psi(\text{ASDWZ}) = \left|\frac{1}{\sqrt{2}}(\phi_2+\phi_3)\frac{1}{\sqrt{2}}(\overline{\phi}_2+\overline{\phi}_3)\psi_1^+\psi_1^-\right|. \tag{23}$$

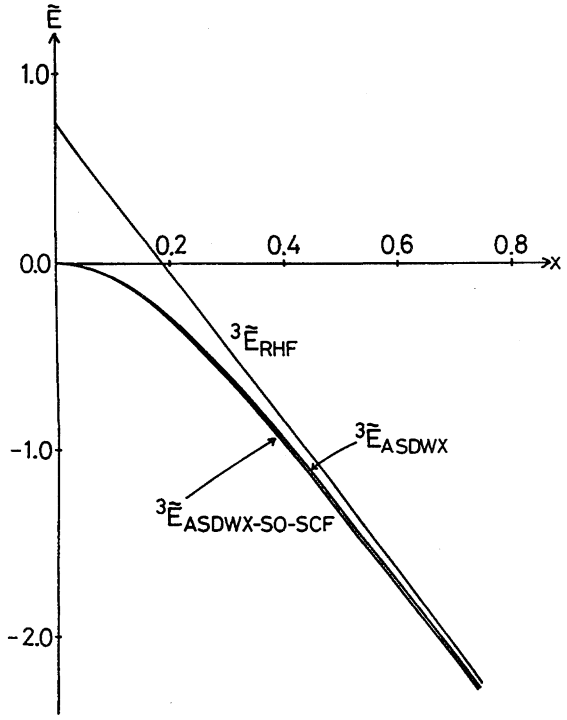

Fig. 6. Normalized energies of the ASDWX-SO-SCF, ASDWX, and RHF states of the triplet state in the D_{4h} conformation. In the T_d conformation. ASDWX is replaced by TSW at the T_d conformation.

The projected ASDWZ solution, therefore, does not involve the semi-internal (SI) configuration in Eq. 19, and therefore PASDWZ solution is less stable than PASDWX. Thus the triplet UHF and PUHF solutions and many other papers do not involve the semi-internal (SI) contribution, which is crucial for stabilization of the triplet state. This is the reason why the conventual UHF theory predicts the greater stability of the singlet state than the triplet state for H_4 radical (**4**), square planar cyclobutadiene (**5**) and Cu_4O_4 cluster (**6**) with the D_{4h} symmetry. The spin polarization (SP) rule was thus derived from the conventual UHF (ASDWZ) model. However, judging from significant difference between the PASDWX and PASDWZ results, the SP rule should be modified to include the semi-internal and external correlation effects if it does not work well in subtle cases.

Figures 7(A) and 7(B) show variations of the optimized orbital mixing parameter λ and spin coupling parameter σ as the functions of x. The λ-value of the PASDWX state is uniformly smaller than that of the SO-SCF state, just as has been the case with the singlet state. However, unlike the case of the singlet state, σ diminishes drastically as x increases.

The tetraradical character y was calculated to be

$$y = \frac{1}{2}\left(\frac{NC_3}{2}\right)^2[\sigma^2\sin^2\lambda + (1-\cos\lambda)^2], \tag{24}$$

whose variation with x is illustrated in Fig. 8. They y-value of the PASDWX state agrees closely with that of the SO-SCF state. It is significant, however, to investigate the respective contributions of the semi-internal ($\Phi^{\text{t}}_{\text{SI}}$) and external pair

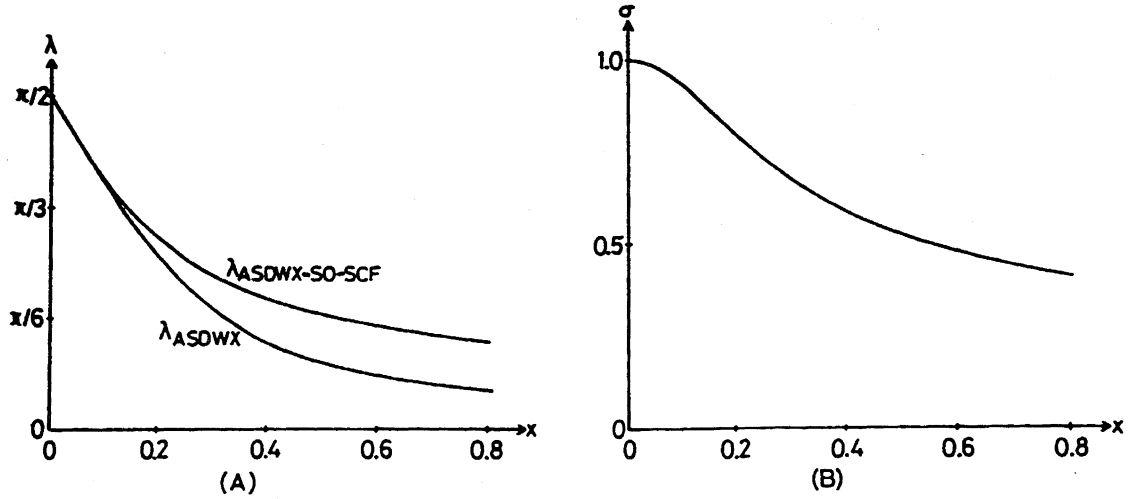

Fig. 7. (A) Variations of the orbital mixing parameter λ with x for the ASDWX-SO-SCF and ASDWX solutions of the triplet state in the D_{4h} conformation. (B) Variation of the spin coupling parameter σ with x for the ASDWX-SO-SCF solution.

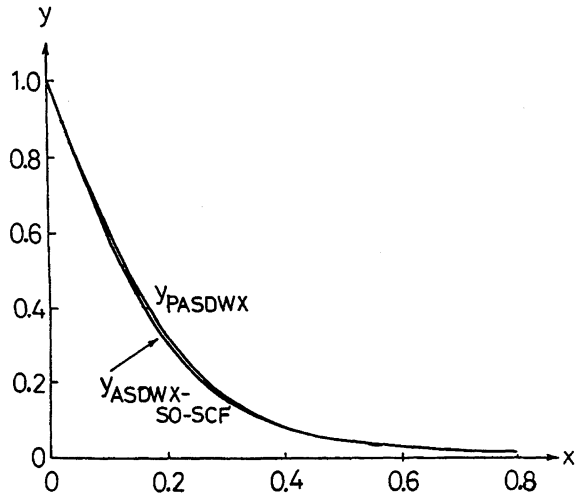

Fig. 8. Tetraradical character of the ASDWX-SO-SCF and PASDWX states of triplet state in the D_{4h} conformation. In the T_d conformation, ASDWX is replaced by TSW.

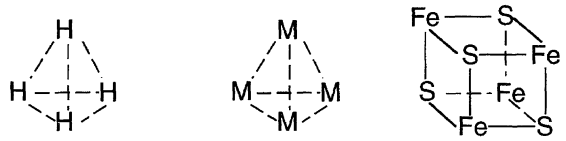

10 **11** **12**

Chart 4.

(Φ_{DE}^{t}) correlation effects.[23] For a fixed x-value, the increase in the λ-value enhances the external pair correlation and semi-internal correlation effects. The semi-internal effects decrease with the increase of σ-value. Compared with the correlation in the SO-SCF solution, the semi-internal correlation effect in PASDWX state is, therefore, overestimated, while the external pair correlation effect is underestimated. This situation is the same as that of the singlet state of the D_{4h} radical. However, since these differences are small, the PASDWX state is regarded as a good trial for the SO-SCF (CASSCF) calculation.[26]

Singlet State in the T_d Conformation (9). There are several model systems with T_d conformation: H_4 cluster (**10**), M_4 cluster (**11**) (M=Li, Na, etc.), Fe_4S_4 cluster (**12**) in ferredoxin, and so on (Chart 4). As a model for **10** and **11**, the Hubbard model for {4,4} system with T_d conformation is examined. The RHF orbitals $\{\phi_i\}$ of the T_d conformation are easily determined by the T_d spatial symmetry (see Eq. 9 of Ref. 16). The orbitals ϕ_2, ϕ_3, and ϕ_4 are triply degenerated and are the bases of the irreducible representation t_2. The most stable solution within the single Slater-determinant approximation is the torsional-spin-wave (TSW) solution (**9**) given by the magnetic double group $\bar{4}'3m$.[32]

$$\psi_1^+ = \left[\phi_1 \cos\frac{\lambda}{2} + \frac{1}{\sqrt{3}}(\sigma_z\phi_2 + \sigma_y\phi_3 + \sigma_x\phi_4)\sin\frac{\lambda}{2}\right]\eta_\pm,$$
$$\psi_2^\pm = \frac{1}{\sqrt{3}}(\sigma_z\phi_2 + \omega^2\sigma_y\phi_3 + \omega\sigma_x\phi_4)\eta_\pm,$$
$$\omega = \exp\left(\frac{2}{3}\pi i\right). \quad (25)$$

The total electronic energy of single Slater determinant constructed from these orbitals is again the same as Eq. 15.

The transformation properties of the TSW solution under an operation of the elements of T_d (for G) are summarized in Table 3. The transformation induces a 2×2 matrix, reflecting the two-component character of the TSW solution. Nevertheless, the spin density derived from the transformed orbitals does not alter. The TSW state is invariant under the elements of the subgroup T and time reversal elements of (T_d–T). Therefore, the TSW solution possesses the symmetry characterized by the magnetic point group $\bar{4}'3m$ (Eq. 4).

The SO-SCF wavefunction is obtained by the projection of the orbital product $\psi_1^+\psi_1^-\psi_2^+\psi_2^-$ on the eigenstate with M=S=0:

$$^1\Psi_{\text{TSW-SO-SCF}} = D_1\Phi_G^s + D_2\Phi_2^s + D_3\Phi_{DE}^s, \quad (26)$$

where

Table 3. Transformation Properties of the TSW Orbitals with the $\bar{4}'3m$ Symmetry[a,b]
One of the Generator Sets is $\{E, C_{2x}, C_{2y}, C^{+}_{31}, C^{-}_{31}, (S^{+}_{4x})^{t}\}$.

	Ψ_1^+	Ψ_1^-	Ψ_2^+	Ψ_2^-
E	Ψ_1^+	Ψ_1^-	Ψ_2^+	Ψ_2^-
C_{2x}	$-i\Psi_1^+$	$-i\Psi_1^-$	$-i\Psi_2^+$	$-i\Psi_2^-$
C_{2y}	Ψ_1^-	$-\Psi_1^+$	Ψ_2^-	$-\Psi_2^+$
C^{+}_{31}	$\frac{\varepsilon}{\sqrt{2}}\sigma_z(\Psi_1^+ + \Psi_1^-)$	$\frac{\varepsilon}{\sqrt{2}}\sigma_z(\Psi_1^+ - \Psi_1^-)$	$\frac{1}{\sqrt{2}}\varepsilon\omega^2\sigma_z(\Psi_2^+ + \Psi_2^-)$	$\frac{1}{\sqrt{2}}\varepsilon^*\omega^2\sigma_z(\Psi_2^- - \Psi_2^-)$
C^{-}_{31}	$\frac{\varepsilon^*}{\sqrt{2}}\sigma_x\sigma_z(i\Psi_1^+ - \Psi_1^-)$	$\frac{\varepsilon^*}{\sqrt{2}}\sigma_x\sigma_z(i\Psi_1^+ + \Psi_1^-)$	$\frac{\varepsilon^*}{\sqrt{2}}\omega\sigma_x\sigma_z(i\Psi_2^+ - \Psi_2^-)$	$\frac{\varepsilon^*}{\sqrt{2}}\omega\sigma_x\sigma_z(i\Psi_2^+ + \Psi_2^-)$
$^t(S^{+}_{4x})$	$-\frac{1}{\sqrt{2}}(i\Psi_1^+ + \Psi_1^-)$	$\frac{1}{\sqrt{2}}(\Psi_1^+ + i\Psi_2^-)$	$-\frac{\omega}{\sqrt{2}}(i\Psi_2^+ - \Psi_2^-)$	$\frac{\omega}{\sqrt{2}}(\Psi_2^+ + i\Psi_2^-)$
$^t(S^{-}_{4x})$	$\frac{1}{\sqrt{2}}(i\Psi_1^+ + \Psi_1^-)$	$\frac{1}{\sqrt{2}}(\Psi_1^+ - i\Psi_1^-)$	$\frac{\omega}{\sqrt{2}}(i\Psi_2^+ - \Psi_2^-)$	$\frac{\omega}{\sqrt{2}}(\Psi_2^+ - i\Psi_2^-)$
$^t(\sigma_{da})$	$\varepsilon^*\sigma_z\Psi_1^+$	$-\varepsilon\sigma_z\Psi_1^-$	$\varepsilon^*\sigma_z\Psi_2^+$	$-\varepsilon\sigma_z\Psi_2^-$

a) $\varepsilon=\exp(\frac{\pi}{4}i)$, $\omega=\exp(\frac{2}{3}\pi i)$. b) t is a time inversion operator.

$$\Phi_G^s = \frac{1}{\sqrt{3}}(|\phi_1\overline{\phi}_1\phi_2\overline{\phi}_2| + \omega|\phi_1\overline{\phi}_1\phi_3\overline{\phi}_3| + \omega^2|\phi_1\overline{\phi}_1\phi_4\overline{\phi}_4|),$$
$$\Phi_2^t = \frac{1}{\sqrt{6}}(|\phi_1\phi_2\overline{\phi}_3\overline{\phi}_4| + |\overline{\phi}_1\overline{\phi}_2\phi_3\phi_4|) + \omega(|\phi_1\overline{\phi}_2\phi_3\overline{\phi}_4| + |\overline{\phi}_1\phi_2\overline{\phi}_3\phi_4|) + \omega^2(|\phi_1\overline{\phi}_2\overline{\phi}_3\phi_4| + |\overline{\phi}_1\phi_2\phi_3\overline{\phi}_4|), \quad (27)$$
$$\Phi_{DE}^s = \frac{1}{\sqrt{3}}(|\phi_3\overline{\phi}_3\phi_4\overline{\phi}_4| + \omega|\phi_2\overline{\phi}_2\phi_4\overline{\phi}_4| + \omega^2|\phi_2\overline{\phi}_2\phi_3\overline{\phi}_3|),$$

and where

$$D_1 = -\frac{C_2N}{\sqrt{3}}\cos^2\frac{\lambda}{2}, \quad D_2 = -\frac{i}{3\sqrt{2}}C_2N\sigma\sin\lambda,$$
$$D_3 = -\frac{C_2N}{3\sqrt{3}}(2\sigma+1)\sin^2\frac{\lambda}{2}, \quad \sigma = C_1/C_2,$$
$$\left(\frac{C_2N}{3}\right)^2 = \left[3\cos^4\frac{\lambda}{2} + \frac{1}{3}(2\sigma+1)^2\sin^4\frac{\lambda}{2} + \frac{\sigma^2}{2}\sin^2\lambda\right]^{-1}. \quad (28)$$

The SO-SCF solution contains the ground (Φ_G^s), pseudo-double-excitation (Φ_2^s) or spin polarization, and double-excitation (Φ_{DE}^s) configurations.

Let us study the space symmetry of each configuration. The configuration Φ_G can be factorized into the real and imaginary parts as follows:

$$\Phi_G^s = \frac{1}{\sqrt{2}}(\Phi_{G1} + i\Phi_{G2}),$$
$$\Phi_{G1}^s = \frac{1}{\sqrt{6}}(2|\phi_1\overline{\phi}_1\phi_2\overline{\phi}_2| - |\phi_1\overline{\phi}_1\phi_3\overline{\phi}_3| - |\phi_1\overline{\phi}_1\phi_4\overline{\phi}_4|),$$
$$\Phi_{G2}^s = \frac{1}{\sqrt{2}}(|\phi_1\overline{\phi}_1\phi_3\overline{\phi}_3| - |\phi_1\overline{\phi}_1\phi_4\overline{\phi}_4|). \quad (29)$$

Since Φ_{G1}^s and Φ_{G2}^s are the basis functions of the irreducible representation e, the space symmetry of Φ_G^s is characterized as ^1E. Similarly, both Φ_2^s and Φ_{DE}^s possess the E-symmetry, because they can be factorized into the real and imaginary parts whose space symmetries are characterized as ^1E. Therefore, the SO-SCF state obtained from the magnetically ordered set $\bar{4}'3m$ has the ^1E-symmetry. There are three irreducible representations e in the singlet state of the T_d conformation. The partner function[27] in each irreducible representation e does not interact with the various configurations given by Eq. 29. Consequently, the SO-SCF wavefunction is identical with the exact full CI solution in the minimal basis approximation and the CASSCF solution in the extended basis set.

The total electronic energy of the SO-SCF state is expressed as

$$^1E_{TSW\text{-}SO\text{-}SCF} = -4x(D_1^2 - D_3^2) + 3(D_2)^2/4 - D_1D_3/2 - \sqrt{6}iD_2(D_1 + D_3)/2 + 3/4. \quad (30)$$

The explicit form for $\sigma=1$ agrees with Eq. 15 for the PASDWZ state of the D_{4h} conformation. Therefore, the TSW-EHF and ASDWZ-EHF states give the same λ-value and energy value. Even when $\sigma\neq1$, the optimized energies obtained from Eqs. 15 and 30 are identical with each other. Thus, the variation of the energy for each state with x is entirely the same as in Fig. 3. The variations of λ and σ are also practically the same as in the D_{4h} conformation (Fig. 4).

The tetraradical character y is calculated to be

$$y = \left(\frac{C_2N}{3}\right)^2\left[\sigma^2\sin^2\lambda + \frac{1}{9}(2\sigma+1)^2(1-\cos\lambda)^2\right]. \quad (31)$$

When $\sigma=1$, Eq. 31 agrees exactly with Eq. 17. The y-value for the case of $\sigma=1$ nearly coincides with the value for the full CI state of the singlet state in the D_{4h} conformation. As a result, Fig. 3 is considered to be valid for the T_d conformation as well. Thus the y-value of the PTSW state is less than that of the SO-SCF state. That the y-value of the EHF state is nearly equal to the SO-SCF state indicates that the total contributions of the correlation effects Φ_2^s and Φ_{DE}^s in the EHF and SO-SCF states are the same. In the EHF state, the weights of the pseudo-double-excitation (Φ_2^s) and double-excitation (Φ_{DE}^s) configurations are greater than those of the PTSW state because of the larger λ-value. In comparison with the TSW-EHF state, the weight of Φ_2^s in the SO-SCF state somewhat decreases while that of Φ_{DE}^s slightly increases. Judging from the full CI (SO-SCF) solution, the correlation effect of the configuration Φ_2^s in the EHF state is a bit too excessive. In the PTSW state, on the other hand, the correlation effects of Φ_2^s and Φ_{DE}^s are underestimated. The situation is the same as those of the singlet and triplet D_{4h} states. Since the correlation corrections for the PTSW state are small, the PTSW state is a good trial for the SO-SCF calculation of the ^1E state in the T_d-conformation.

The real part Φ_{G1}^s and imaginary part Φ_{G2}^s of the configuration Φ_G^s possess respectively the symmetries $^1A_1$ and $^1B_1$

of the point group D_{2d} which is the subgroup of T_d. Since the configurations Φ_2^s and Φ_{DE}^s exhibit the same property as does the configuration Φ_G^s, the SO-SCF wavefunction is rewritten as

$$^1\Psi_{TSW\text{-}SO\text{-}SCF}(^1E) = \Phi(^1A_1) + i\Phi(^1B_1), \tag{32}$$

where $\Phi(^1A_1)$ is the ground state in the extended D_{2d} conformation, while $\Phi(^1B_1)$, which is more stable than $\Phi(^1A_1)$ in the compressed D_{2d} conformation, is connected with the $^1B_{1g}$-state in the D_{4h} conformation. In the T_d-conformation, $\Phi(^1A_1)$ and $\Phi(^1B_1)$ are degenerate with each other.

Triplet State in the T_d Conformation. After the orbital product $\psi_1^+\psi_1^-\psi_2^+\psi_2^-$ has been projected on the component with M=0, the SO-SCF wavefunction of the triplet state is given as

$$^3\Psi_{TEW\text{-}SO\text{-}SCF} = D_1\Phi_{GT}^t + D_2\Phi_2^t + D_3\Phi_{DE}^t, \tag{33}$$

where

$$\begin{aligned}
\Phi_G^t &= \frac{1}{\sqrt{2}}(|\phi_1\overline{\phi}_1\phi_3\overline{\phi}_4| + |\phi_1\overline{\phi}_1\overline{\phi}_3\phi_4|),\\
\Phi_2^t &= \frac{1}{2}(|\phi_1\overline{\phi}_2\phi_4\overline{\phi}_4| + |\overline{\phi}_1\phi_2\phi_4\overline{\phi}_4|\\
&\quad - |\phi_1\overline{\phi}_2\phi_3\overline{\phi}_3| - |\overline{\phi}_1\phi_2\phi_3\overline{\phi}_3|),\\
\Phi_{DE}^t &= \frac{1}{\sqrt{2}}(|\phi_2\overline{\phi}_2\phi_3\overline{\phi}_4| + |\phi_2\overline{\phi}_2\overline{\phi}_3\phi_4|),
\end{aligned} \tag{34}$$

and where

$$\begin{aligned}
&D_1 = \frac{\sqrt{2}}{3}iNC_3\cos^2\frac{\lambda}{2}, \quad D_2 = -\frac{i}{3}NC_3\sigma\sin\lambda,\\
&D_3 = -\frac{\sqrt{2}}{9}iNC_3(2\sigma+1)\sin^2\frac{\lambda}{2},\\
&\left(\frac{NC_2}{3}\right)^2 = \left[2\cos^4\frac{\lambda}{2} + \frac{2}{9}(2\sigma+1)^2\sin^4\frac{\lambda}{2} + \sigma^2\sin^2\lambda\right]^{-1},\\
&\sigma = \frac{C_1}{C_3} = \frac{C_2}{C_3}.
\end{aligned} \tag{35}$$

The resulting SO-SCF wavefunction contains the ground (Φ_G^t), pseudo-double-excitation (Φ_2^t), and double-excitation (Φ_{DE}^t) configurations. The SO-SCF wavefunction is identical to the exact full CI solution within the minimal basis approximation, because three t_1-representations are contained in the triplet state and the partner functions of the t_1-representation do not interact with the configurations Φ_G^t, Φ_2^t, and Φ_{DE}^t. Consequently, the projection of the TSW solution with $\overline{4}'3m$ symmetry on the triplet state with M=0 produces the exact full CI solution without the healing of the space symmetry.

The total electronic energy of the SO-SCF state is expressed in terms of the CI coefficients as

$$\begin{aligned}
^3E_{TSW\text{-}SO\text{-}SCF} &= -4x(|D_1|^2 - |D_3|^2) - |D_2|^2/4 + D_1D_3^*\\
&\quad + 2D_2^*(D_1 - D_3) + 3/4.
\end{aligned} \tag{36}$$

When σ=1, this equation reduces to Eq. 23. Accordingly, the PTSW and TSW-EHF states are the same. The energy of the EHF state is equal to that of the D_{4h} conformation due to the same optimized λ-value as that of the D_{4h} conformation. Even though λ- and σ-values differ from those of the D_{4h} conformation, the energy is identical with that for the SO-SCF state of the D_{4h} conformation. Thus, the energy profiles of the triplet state in the T_d conformation are exactly the same as given in Fig. 6. It follows that the ground state of the T_d conformation is the singlet state.[8)]

The variations of the optimized λ- and σ- values and of the tetraradical character y with x are essentially the same as those for the triplet state in the D_{4h} conformation (Figs. 7 and 8).

The space symmetry of the SO-SCF wavefunction is reduced to the $^3A_2$ symmetry by the subduction to the subgroup D_{2d}. This state, which is the lowest triplet in the compressed D_{2d} conformation, is connected with the $^3A_{2g}$ state in the D_{4h} conformation. The $^3A_2$ and ^3E states are mutually degenerate in the triplet state of the T_d conformation.

Triplet State in the D_{3h} Conformation. The triplet state of the D_{3h} conformation is interesting in relation to the triplet state of the trimethylene methane analogs as shown in Fig. 9. The RHF orbitals $\{\phi_i\}$ are determined by the D_{3h} symmetry of the system (see Eq. 17 of Ref. 16). Figures 9B and 9C illustrate the RHF HOMO (ϕ_1) and LUMO (ϕ_4). The instability condition provides an ASDWZ solution.[16)]

$$\begin{aligned}
&\psi_1^{\pm} = \left[\left(\cos\frac{\lambda}{2}\right)\phi_1 \pm \left(\sin\frac{\lambda}{2}\right)\phi_4\right]\eta_{\pm},\\
&\psi_2^+ = \phi_e\eta_+, \quad \psi_3^+ = \phi_{-e}\eta_+.
\end{aligned} \tag{37}$$

The DODS MOs ($\psi_1^{\pm}$) in Eq. 37 are also shown in Figs. 9D and 9E, together with the spin densities. The ASDWZ solution is kept invariant under the symmetry operations of $C_{3h}+T(D_{3h}-C_{3h})$. Thus the ASDWZ solution possesses the full magnetic symmetry characterized as $\overline{6}\,m'\,2'$. The corresponding spin structure is depicted in Fig. 9F. The SO-SCF wavefunction is similarly derived as in the case of the triplet state of the D_{4h} and T_d conformations. Thus,

$$^3\Psi_{ASDWZ\text{-}SO\text{-}SCF} = D_1\Phi_G^t + D_2\Phi_{SP}^t + D_3\Phi_{DE}^t, \tag{38}$$

where

$$\begin{aligned}
\Phi_G^t &= |\phi_1\overline{\phi}_1\phi_e\,\phi_{-e}|,\\
\Phi_{SP}^t &= \frac{1}{2}(|\phi_1\,\phi_e\,\phi_{-e}\overline{\phi}_4| - |\overline{\phi}_1\phi_e\,\phi_{-e}\phi_4|\\
&\quad - |\phi_1\,\phi_e\,\overline{\phi}_{-e}\phi_4| + |\phi_1\overline{\phi}_e\phi_{-e}\phi_4|),\\
\Phi_{DE}^t &= |\phi_e\,\phi_{-e}\phi_4\overline{\phi}_4|,
\end{aligned} \tag{39}$$

and where

$$\begin{aligned}
&D_1 = -\frac{NC_3}{2}\cos^2\frac{\lambda}{2}, \quad D_2 = -\frac{-NC_3}{4}\sigma\sin\lambda,\\
&D_3 = -\frac{NC_3}{2}\sin^2\frac{\lambda}{2}, \quad \left(\frac{C_3N}{2}\right)^2 = \left[1 + \frac{1}{4}(\sigma^2-2)\sin^2\lambda\right]^{-1}.
\end{aligned} \tag{40}$$

The ground (Φ_G^t), spin-polarization (Φ_{SP}^t), and double-excitation (Φ_{DE}^t) configurations are generated. All the three configurations possess the common space symmetry A_2'. There exist four configurations characterized as the A_2'-symmetry. The residual configuration does not interact with the other three configurations in the present model. Thus the SO-SCF

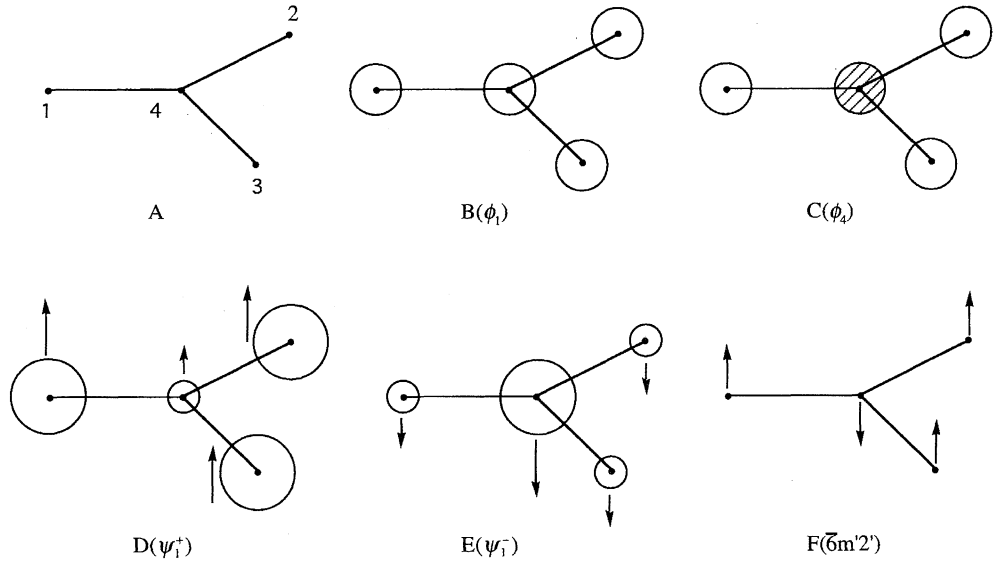

Fig. 9. The molecular structure of the D_{3h} radical (A), trimethylene methane analog (B) and spin structure with the full magnetic symmetry ($\bar{6}\,m'\,2'$).

wavefunction should give the results identical with the full CI within the minimal basis approximation.

The total electronic energy of the SO-SCF state is given as

$$^3\tilde{E}_{\text{ASDWZ-SO-SCF}} = -2\sqrt{3}x(D_1^2 - D_3^2) + \frac{2}{3}(D_1D_2 - D_2D_3 + D_3D_1) + \frac{2}{3}. \quad (41)$$

The energies of the PASDWZ and EHF states correspond to the case where $\sigma=1$:

$$^3E_{\text{PASDWZ}} = \frac{-8\sqrt{3}x\cos\lambda}{3+\cos^2\lambda} - \frac{2\sin\lambda}{3(2-\sin\lambda)} + \frac{2}{3}. \quad (42)$$

Functional dependence of the reduced energies on x is shown in Fig. 10. The SO-SCF state is seen to be well approximated by the ASDWZ state in terms of energy.

Variations of the orbital mixing parameter λ and spin coupling parameter σ with x are much the same as those found for the D_{4h} triplet state (Fig. 7). The tetraradical character y calculated for the PASDWZ, SO-SCF and EHF states, are illustrated in Fig. 11. In the PASDWZ state, both the spin-polarization and double-excitation effects are underestimated, while in the EHF state, the spin polarization effect is overestimated. Since the correlation corrections are small, the PASDWZ state is a good trial to obtain the correlated wavefunction with correct symmetries. Thus the characteristics of several solutions for the triplet D_{3h} radical are similar in other cases examined above.

The Energy Hypersurfaces of the SCF Processes

The results obtained in the preceding sections are summarized in Table 4. The third and fourth columns show the magnetically ordered solutions and their magnetic symmetries, respectively. The final column indicates the space symmetries of the SO-SCF solutions generated from the magnetically ordered solutions.

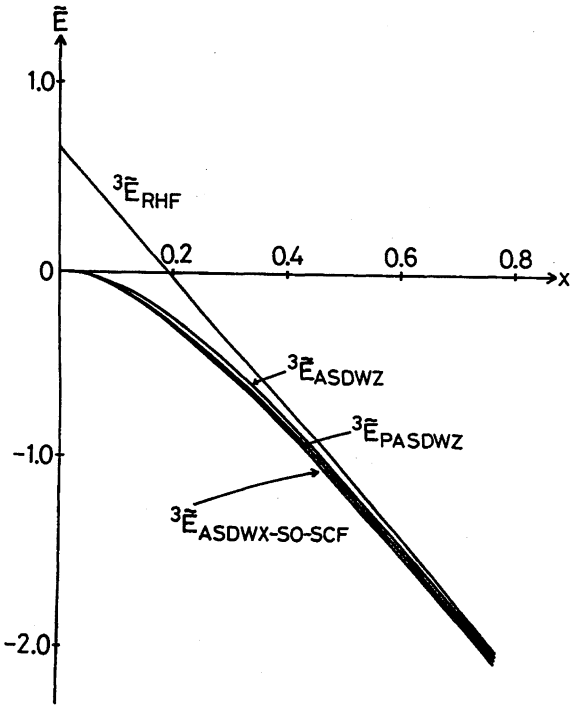

Fig. 10. Normalized energies of the ASDWZ, PASDWZ, and RHF solutions of the triplet state in the D_{3h} conformation.

Every SO-SCF wavefunction obtained here satisfies the space symmetries. This is due to the fact that a spin-symmetry breaking solution, which consists of the basis functions of the point group, possesses the symmetry characterized by the magnetic point group based on the point group (P_N).[23]

In addition, the tensor products of orbitals ϕ_1, ϕ_2, ϕ_3, and ϕ_4 arising from the S_z^M component of the orbital product contain the common space symmetry due to the reduction by permutation group.

The energy of the SO-SCF wavefunction is dependent on

Table 4. The SO-SCF (Full CI) States of Four-Electron Systems

Point group	Spin symmetry	HF solution	Magmetic piont group	Space symmetry of the SO-SCF state
D_{4h}	Singlet	ASDWZ	4′/mmm′	$^1B_{1g}$
	Triplet	ASDWX	m′m′m	$^3A_{2g}$
T_d	Singlet	TSW	$\overline{4}'3m$	^1E
	Triplet	TSW	$\overline{4}'3m$	$^3T_1$
D_{3h}	Triplet	ASDWZ	$\overline{6}m'2'$	$^3A_2'$

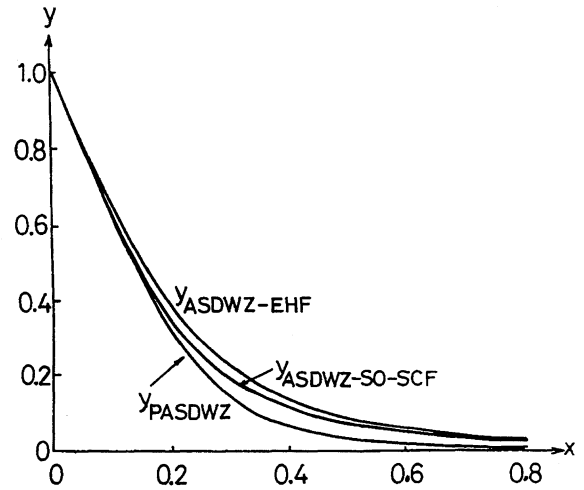

Fig. 11. The tetraradical characters of the ASDWZ-SO-SCF, ASDWZ-EHF, and PASDWZ states of the triplet state in the D_{3h} conformation.

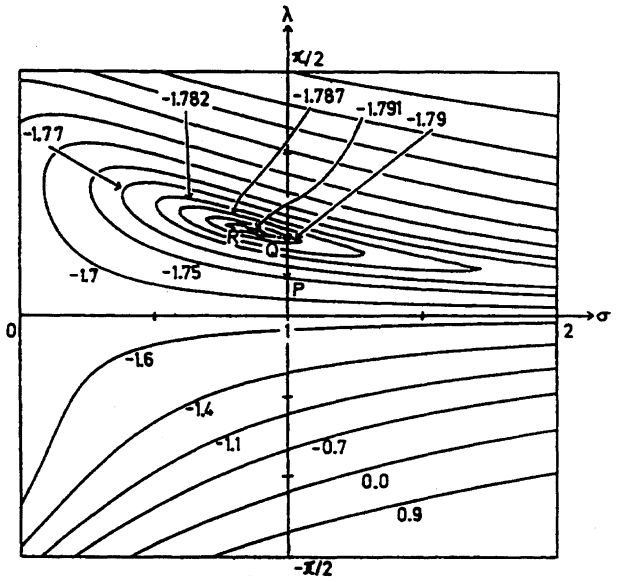

Fig. 12. The energy surface as a function of the orbital mixing (λ) and spin coupling (σ) parameters at x=0.6 for the singlet state in the T_d conformation. The points P, Q, and R on the surface correspond to the PTSW, TSW-EHF, and TSW-SO-SCF (full CI) states, respectively. The figures appended to the contour lines indicated the reduced energy.

two variables, i.e., the orbital mixing parameter λ and spin coupling parameter σ. Figure 12 shows the energy contour map of the singlet state of the T_d configuration. The state obtained by Löwdin's projection[20c] lies on the line of σ=1. The point P and Q correspond to the PTSW and TSW-EHF states, respectively. The PTSW state (P) is situated on a slanting surface. The EHF state (Q) falls on a kind of saddle point rather than a local minimum. Therefore, it is easy to arrive at the TSW-EHF state from the PTSW state along the line σ=1. When we go to the SO-SCF state (R) from the TSW-EHF state, there is no energy barrier which we have to overcome. In other words, the PGHF state is a good starting point to get the full CI (SO-SCF) state by direct minimization. It follows that the path TSW→PTSW→TSW-EHF→SO-SCF is a good trial to reach the absolute minimum. Eventually, therefore, the TSW solution obtained by the stability analysis of the RHF solution is a good trial point to locate the exact solution for the T_d conformation. Since the energy behavior of the TSW state is similar to that of the SO-SCF state, the TSW solution itself is a good approximation to the SO-SCF state in terms of energy, although it is symmetry-broken.

Similar results are expected with the triplet state of the D_{3h} conformation. The energy contour map at x=0.5 is shown in Fig. 13. Here also, the EHF state (Q) is situated on a saddle-like point. The EHF state smoothly connects with the

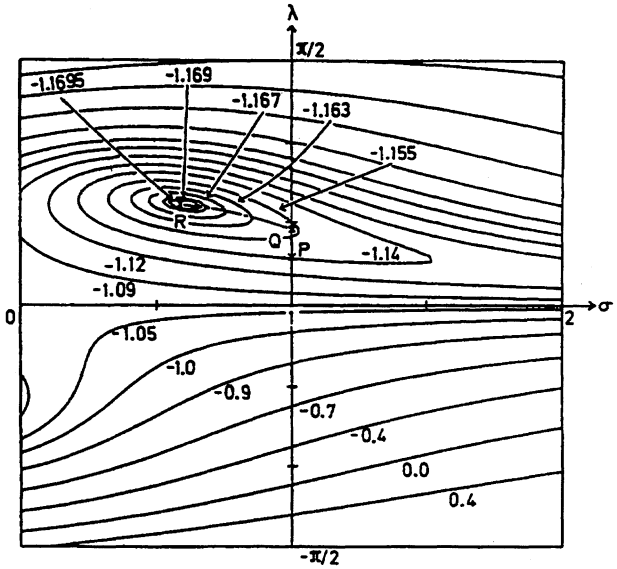

Fig. 13. The energy surface as a function of the orbital mixing (λ) and spin coupling (σ) parameters at x=0.5 for the triplet state in the D_{3h} conformation. The points P, Q, and R on the surface correspond to the PASDWZ, ASDWZ-EHF, and ASDWZ-SO-SCF (full CI) states, respectively. The figures appended to the contour lines indicate the reduced energy.

absolute minimum (R) corresponding to the SO-SCF (full CI) state without the energy barrier on the way. Therefore, the ASDWX solution is a good starting point to get to the full CI state.[26] It has been confirmed that the situation is also true in the remaining cases.

Discussions and Concluding Remarks

Interrelationships between Model Hamiltonians. In a previous paper,[25b] we have thoroughly investigated the interrelationships between the unrestricted Hartree–Fock (UHF), namely ASDWZ in this paper, UHF natural orbital (NO) CI, UNO CASSCF and CASPT2 methods in the case of 1, 3-dipoles and -biradicals. Since such ab initio treatments of multicenter transition-metal clusters are not so easy, we have here considered Hubbard and Heisenberg models for four-center four-electron {4,4} systems with D_{4h}, T_d, and D_{3h} conformations to elucidate characteristics of spin and electron correlation effects in these species. The analytical expressions of the energy and CI coefficients can be derived in these models, and they have indeed revealed common characteristics for several wavefunctions used for elucidation of antiferromagnetic correlation and derivation of spin alignment rules as follows:

(1) The spin-density-wave (SDW) type Hartree–Fock (HF) solutions with axial, helical, and torsional spin modulations are derived from the instability analysis of the restricted HF (RHF) solution.

(2) The projected SDW solutions involve all the configurations which are necessary for the spin-restricted full CI calculations, while the SDW solutions involve all these terms, together with other spin contamination contributions.

(3) The projected SDW solutions are good trials for the spin-optimized (SO) SCF solutions which are equivalent to the full CI within active magnetic orbitals.

(4) The SDW and spin-projected SDW solutions usually overestimate the contribution of the spin polarization (SP) configuration but underestimate the contribution of the double excitation (DE) configuration, as compared with the corresponding results obtained by the full CI solution.

From these results, we have practical procedures to elucidate complex spin correlations and spin alignments on the basis of the model Hamiltonians given in Fig. 1:

(a) The spin vector model or classical Heisenberg model is applied to elucidate possible spin alignments for radical species and the magnetic symmetries ($T\times S$) of the spin structures.

(b) The Hückel and/or extended Hückel calculations are performed for molecular systems to elucidate the energy gaps between magnetic orbitals, and their spatial symmetries (P_N). If the energy gaps exceed a threshold value, the species under consideration are usually nonradical species or low-spin species.

(c) The SDW solutions are constructed from the magnetic double group ($T\times S\times P_N$) in combinations with the above results (a) and (b). The spin densities obtained from these solutions are utilized to depict the spin alignments (or spin correlation functions).

(d) However, it is noteworthy that the SDW solutions do not provide real spin densities of small clusters, in contrast with infinite systems with three-dimensional lattices.

(e) The spin projection of SDW solutions provides important spin-restricted configurations, leading to qualitative explanation of spin correlations and mechanisms of spin alignments in molecular magnetic materials.

(f) If necessary, the limited CI, SO-SCF, and CASSCF calculations[26] are performed to confirm such qualitative explanations at step (e) and to obtain more refined quantitative results, such as the weights of spin polarization and other electron correlation configurations, spin densities, and so on.

Reduction to Spin Hamiltonians. According to the above theoretical procedures, we can obtain CASSCF solutions for magnetic clusters unless the number of active magnetic natural orbitals becomes over fifteen. However, such ab initio computations are impossible for larger magnetic clusters with even larger CAS. Therefore, the Heisenberg models in Fig. 1 are often utilized for qualitative discussions of molecular magnetism. For example, the present Hubbard model for the four-center four-electron {4,4} system is reduced to the Heisenberg model with the four-site four-spin (S=1/2) system if the intersite resonance integral ($|\beta|$) in Eq. 10 is much smaller than the on-site repulsion integral (U). Under the condition ($|\beta|\gg U$), the interatomic interactions are expressed by the effective exchange integrals between localized spin orbitals i and j.

$$J_{ij} = -\frac{2\beta^2}{U} = -2Ux^2 \tag{43}$$

where, x is defined by Eq. 10.

The J_{ij}-value is about -1000 cm^{-1} for the nearest neighbor spins on the copper atoms of the copper oxide unit (**6**) with axial spin structure (**7**). The spin state of the two-dimensional (2D) lattice in La_2CuO_4 and related copper oxides is well described by the Heisenberg model. The Heisenberg model is also applied to a fifteen-oxovanadium cluster (**13**) (Chart 5), $K_6[V_{15}As_6O_{42}(H_2O)]\cdot 8H_2O$, where V(IV) has a spin (S=1/2). **13** has a magnetic multilayer structure with antiferromagnetic layers sandwiching a triangular lattice with

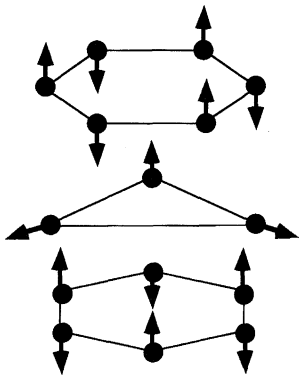

13

Chart 5.

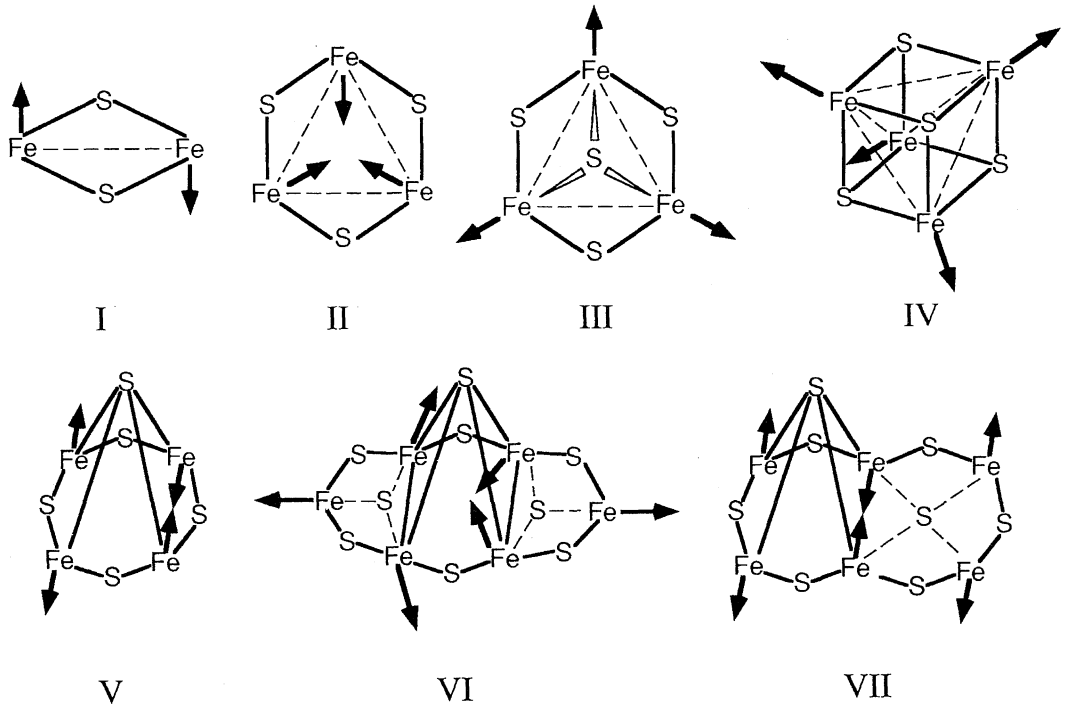

Fig. 14. The spin structures (**I**—**VII**) obtained for iron-sulfur clusters (see Table 5) by the Heisenberg model.

helical spin structure (**3**).[34] This spin structure (**13**) is easily obtained since the effective exchange interactions are considered only for nearest neighbor sites.

The Heisenberg model can be extended to more complex systems involving transition metal ions. The effective exchange integrals between transition metal ions are usually described by an orbital average form as

$$J_{ab} = \frac{1}{m \times n} \sum_{i=1}^{m} \sum_{j=1}^{n} J_{ij}, \tag{44}$$

where a and b sites have the m- and n-magnetic orbitals, respectively. The Heisenberg model for multi-center multi-electron systems are, therefore, given by Eq. 1, and spins are often treated as classical spins as shown in Eq. 2 since $s \geq 1$. For example, the Heisenberg model is applicable to the antiferromagnetic square planar Mn(II) cluster, for which Cu(II) in **6** is replaced by Mn(II) (S_a=5/2). This means that the twenty-orbital twenty-electron {20,20} system presented by the Hubbard model is reduced to the four-center four-spin system with the orbital average effective exchange integrals (J_{ab}). It is noteworthy that the size of spins in Eq. 2 is given by the average values for mixed-valence (MV) spin pairs such as the Mn(III)–Mn(IV) pair (S_a=S_b=3.5/2).[35]

Applications to Iron–Sulfur Clusters. As an example of the present procedures in Fig. 1, let us consider ferredoxin systems[34] with the Fe_4S_4 cores (**12**), which have the T_d and D_{2d} conformations:

Table 5. The Molecular Structures (Sym.), Spin State (S), and Oxidation Numbers (o. n.) of Irons and Effective Exchange Integrals (J) for Iron–Sulfur Clusters

						J-values	
System	m	Sym.	S	MV	o.n.	obsd	calcd
I $[Fe_2S_2]^m$	+2	D_{2h}	0(AF)	2Fe(+3)	3.0	−148, −185	−171,[c] −265[d]
	+1		1/2	Fe(+3),Fe(+2)	2.0,3.0	−70, −110	
II $[Fe_3S_3]^m$	+3	C_{3v}	1/2	3Fe(+3)	3.0	−21, −24	−76
	+2	C_{3v}, C_{2v}	1,2	2Fe(+3),Fe(+2)	2.5,3.0		
III $[Fe_3(\mu_3\text{-S})]^m$	+1	C_{3v}	1/2	3Fe(+3)	2.0		
	0	C_{3v}, C_{2v}	1,2	2Fe(+3),Fe(+2)	2.5,3.0		
IV $[Fe_4S_4]^m$	+3	D_{2d}, C_{2v}	1/2	3Fe(+3),Fe(+2)	2.67		
	+2	D_{2d}	0(AF)	2Fe(+3),Fe(+2)	2.5	−232[a]	−188
	+1	D_{2d}, C_{2v}	1/2	Fe(+3),3Fe(+2)	2.25	−20[b]	
V $[Fe_4S_5]^m$	+2	C_{4v}	0(AF)	4Fe(+3)	3.0		
VI $[Fe_6S_9]^m$	−2	C_{2v}	0(AF)	4Fe(+3),2Fe(+2)	2.67		
VII $[Fe_6S_8]^m$	+2		0(AF)	6Fe(+3)	3.0		

a) J_{obs}(+3,+3)=−275, J_{obs}(+3,+2)=−250, and J_{obs}(+2,+2)=−225, b) J_{obs}(+3,+2)=−60, J_{obs}(+2,+2)=−40 (cm^{-1}), (Ref. 38), c) Ref. 33, d) Ref. 34.

(a) For example, the most general spin structure in Fig. 2C is realized from the T_d-space symmetry.

(b) The EHMO calculations have already revealed the energy levels of T_d symmetry-adapted MOs. Judging from the near degeneracy between HOMO ($4e$) and LUMO ($4t_1$), one can conclude that the triplet instability occurs, in conformity with the temperature-dependent paramagnetism.

(c) The possible spin structures are derived from the magnetic group considerations ($G=T\times S\times P_N$).

(d) The possible GHF solutions are constructed in conformity with the magnetic double group theory. From the t_2-instability, four GHF solutions result, and two of them exhibit the torsional spin structure in Fig. 2C.

(e) Though these general spin structures are nothing but antiferromagnetic spin correlations in a single cluster, the extended systems or clusters of the Fe_4S_4 cluster are considered to accomplish helical and torsional spin arrangements in the solid state.[34]

In the past decade, several iron-sulfur cluster have been synthesized, as summarized in Table 5. The spin alignments in these clusters are easily determined by using the classical Heisenberg model given by Eq. 2. Figure 14 illustrates the spin structures (**I**—**VII**) obtained for the corresponding iron–sulfur clusters in Table 5. From Fig. 14, the iron–sulfur clusters exhibit complex spin correlations expressed by axitial, helical, and torsional spin structures. Thus, the electronic structures of iron–sulfur clusters are labile since several frontier electrons do not form tight pairs, in contrast to those in stable transition-metal clusters satisfying the 18-electron rule. This may in turn indicate that electronic properties, for example oxidation–reduction potentials, of the clusters are sensitive even to variations in local environments such as changes of conformations of thiolate ligands in ferredoxins.[35]

According to the spin structures in Fig. 14, we can construct the GHF solutions for the clusters in conformity with the procedures in Fig. 1. For example, the ab initio AS-DWZ solutions were obtained for both low- and high-spin states of the 2Fe–2S model cluster (**I**).[35] The J_{ab} value in the Heisenberg model (Eq. 1) was calculated to be -171 cm^{-1} by using the total energies of these solutions. It is compatible with the observed value shown in Table 5. Ab initio calculations of larger Fe–S clusters are in progress. On the other hand, the density functional (DFT) calculations of 2Fe–2S[36] and 4Fe–4S[37] clusters have been carried out to elucidate orbital energy levels and J_{ab} values. Since the DFT solutions are limited to the axial SDW-type because of density approximation,[38] only the single J_{ab} value has been obtained for 4Fe–4S[37] clusters, though three J_{ab} values have been experimentally required to explain the magnetic behavior;[39] note that the torsional spin structure becomes the ground state in this situation.[35] Thus ab initio GHF calculations of 4Fe–4S[37] clusters are desirable for distinction between DFT and GHF.

Recently a large Fe–S cluster (**13**), $[Na_2Fe_{18}S_{30}]^{8-}$, was synthesized.[40] It has a cyclic structure, namely disk-like or toroidal topology. The χ^M vs. T plot is indicative of an antiferromagnetic behavior with a singlet ground state, in consistent with Mössbauer results.[40] The magnetic moment per Fe atom at 304 K ($\mu_{Fe}=1.40$ μ_B) is closely comparable with those of other smaller Fe–S clusters in Table 5. The spin orientation of **14** can be understood by the combinations of general spin structures in Fig. 14. Although the GHF solutions for **14** are hard to obtain even at the semiempirical level, the spin orientations can be qualitatively described by the classical Heisenberg models in combination with the magnetic group as shown in Fig. 1. In conclusion, giant transition-metal clusters are of great interest from the viewpoint of molecular magnetism as well as bioinorganic chemistry.[41]

We wish to thank Professors A. Nakamura and N. Ueyama for their helpful discussions. We are also gratefully acknowledge the financial support of the Ministry of Education, Since, Sports and Culture (Grand-in-Aid for Scientific Research on Priority Areas Nos. 283 and 282).

References

1) J. Hubbard, *Proc. R. Soc., Ser. A*, **A276**, 238 (1963).
2) K. Yamaguchi, T. Fueno, and H. Fukutome, *Chem. Phys. Lett.*, **22**, 461 (1973).
3) a) F. A. Matsen, *J. Phys. Chem.*, **68**, 3282 (1964); b) F. A. Matsen, *Int. J. Quantum Chem.*, **10**, 511 (1976).
4) a) K. Yamaguchi, *Chem. Phys. Lett.*, **28**, 93 (1974); b) K. Yamaguchi, *Chem. Phys.*, **25**, 215 (1977).
5) L. Salem, in "Electrons in Chemical Reactions: First Principles," John Wiley & Sons, New York (1982), Chap. 7.
6) A. A. Ovchinnikov, *Theor. Chim. Acta*, **47**, 297 (1978).
7) Y. Yoshioka, K. Yamaguchi, and T. Fueno, *Theor. Chim. Acta*, **45**, 1 (1978).
8) a) K. Yamaguchi, *Chem. Phys. Lett.*, **30**, 288 (1975); b) K. Yamaguchi, *Chem. Phys. Lett.*, **34**, 434 (1975).
9) K. Yamaguchi, Y. Yoshioka, and T. Fueno, *Chem. Phys.*, **20**, 171 (1977).
10) C. J. Bradley and A. P. Cracknell, "The Mathematical Theory of Symmetry in Solids," Clarrendon Press, 1972.
11) W. G. Penney, *Proc. R. Soc., Ser. A*, **A158**, 306 (1937).
12) K. Yamaguchi, *Chem. Phys.*, **29**, 117 (1978).
13) K. Yamaguchi, *Chem. Phys. Lett.*, **35**, 230 (1975); **33**, 330 (1975).
14) J. Cizek and J. Paldus, *J. Chem. Phys.*, **47**, 4976 (1976).
15) K. Yamaguchi and T. Fueno, *Chem. Phys. Lett.*, **38**, 47 and 52 (1976).
16) Y. Yoshioka, K. Yamaguchi, and T. Fueno, *Mol. Phys.*, **35**, 33 (1978).
17) A. W. Overhauser, *Phys. Rev.*, **128**, 1437 (1962).
18) a) H. Fukutome, *Prog. Theor. Phys.*, **52**, 115 (1974); b) M. Ozaki, *Prog. Theor. Phys.*, **67**, 83 (1982).
19) K. Yamaguchi and H. Fukutome, *Prog. Theor. Phys.*, **54**, 1599 (1975).
20) a) U. Kalder and F. E. Harris, *Phys. Rev.*, **183**, 1 (1969); b) R. C. Lander and W. A. Goddard, III, *J. Chem. Phys.*, **51**, 1073 (1969); c) P.-O. Lowdin and O. Goscinski, *Int. J. Quantum Chem.*, **3S**, 533 (1970); d) S. Lunell, *Phys. Rev.*, **A1**, 360 (1970); e) A. Laforgue, J. Cizek, and J. Paldus, *J. Chem. Phys.*, **59**, 2560 (1973).
21) K. Yamaguchi, Y. Yoshioka, and T. Fueno, *Chem. Phys. Lett.*, **46**, 360 (1976).

22) K. Takatsuka, S. Nagase, K. Yamaguchi, and T. Fueno, *J. Chem. Phys.*, **67**, 2527 (1977).
23) K. Yamaguchi, Y. Yoshioka, T. Takatsuka, and T. Fueno, *Theor. Chim. Acta*, **48**, 185 (1978).
24) a) K. Yamaguchi, K. Ohta, S. Yabushita, and T. Fueno, *Chem. Phys. Lett.*, **49**, 555 (1977); b) K. Yamaguchi, S. Yabushita, O. Minokawa, and T. Fueno, *Chem. Phys. Lett.*, **59**, 303 (1978).
25) K. Yamaguchi, *Int. J. Quantum Chem.*, **S14**, 269 (1980); b) Y. Yoshioka, D. Yamaki, G. Maruta, T. Tsunesada, K. Takada, T. Noro, and K. Yamaguchi, *Bull. Chem. Soc. Jpn.*, **69**, 3395 (1996).
26) a) G. Das and A. C. Wahl, *J. Chem. Phys.*, **44**, 87 (1966); b) P. J. Hay, W. J. Hunt, and W. A. Goddard, III, *J. Chem. Phys.*, **57**, 738 (1972); c) B. Roos, *Int. J. Quantum Chem.*, **S14**, 175 (1980); d) P. Pulay and T. P. Hamilton, *J. Chem. Phys.*, **88**, 4926 (1988); e) J. M. Bofill and P. Pulay, *J. Chem. Phys.*, **90**, 3657 (1989).
27) E. P. Wigner, "Group Theory and Its Application to the Quantum Mechanics of Atomic Spectra," Academic Press, New York (1959).
28) T. Yamanouchi, *Proc. Phys. -Math. Soc. Jpn.*, **19**, 436 (1937).
29) M. Kotani, A. Amemiya, E. Ishiguro, and T. Kimura, "Tables of Molecular Integrals," Maruzen Co., Tokyo (1955).
30) M. Kotani, *J. Phys. Soc. Jpn.*, **19**, 2150 (1964).
31) M. Rubinstein and I. Shavitt, *J. Chem. Phys.*, **51**, 2104 (1969).
32) H. Fukutome, M. Takahashi, and T. Takabe, *Prog. Theor. Phys.*, **53**, 1580 (1975).
33) A.-L. Barra, D. Gatteschi, L. Pardi, A. Muller, and J. Dorning, *J. Am. Chem. Soc.*, **114**, 8509 (1992).
34) a) A. Yoshimori, *J. Phys. Soc. Jpn.*, **14**, 807 (1959); b) T. Nagamiya, *Solid State Phys.*, **20**, 305 (1968).
35) a) K. Yamaguchi, T. Fueno, N. Ueyama, A. Nakamura, and M. Ozaki, *Chem. Phys. Lett.*, **164**, 210 (1989); b) K. Yamaguchi, T. Fueno, M. Ozaki, N. Ueyama, and A. Nakamura, *Chem. Phys. Lett.*, **164**, 210 (1989).
36) J. G. Norman, Jr., P. B. Ryan, and L. Noodleman, *J. Am. Chem. Soc.*, **102**, 4279 (1980).
37) A. Aizman and D. A. Case, *J. Am. Chem. Soc.*, **104**, 3267 (1982).
38) N. D. Lang, *Solid Sate Phys.*, **20**, 305 (1968).
39) a) G. C. Papaefthymiou, E. J. Laskowski, S. Frota-Pessoa, R. B. Frankel, and R. H. Holm, *Inorg. Chem.*, **21**, 1723 (1982); b) J. Zhou, Z. Hu, E. Munick, and R. H. Holm, *J. Am. Chem. Soc.*, **118**, 1966 (1996).
40) J.-F. You, B. S. Snyder, G. C. Papaefthymiou, and R. H. Holm, *J. Am. Chem. Soc.*, **112**, 1067 (1990).
41) M. Nishino, S. Yamanaka, Y. Yoshioka, and K. Yamaguchi, *J. Phys. Chem. A*, **101**, 705 (1997).